Article

Bayesian Linear Regression and Natural Logarithmic Correction for Digital Image-Based Extraction of Linear and Tridimensional Zoometrics in Dromedary Camels

Carlos Iglesias Pastrana [1], **Francisco Javier Navas González** [1,2,*], **Elena Ciani** [3], **María Esperanza Camacho Vallejo** [2] and **Juan Vicente Delgado Bermejo** [1]

[1] Department of Genetics, Faculty of Veterinary Sciences, University of Córdoba, 14014 Córdoba, Spain
[2] Andalusian Institute of Agricultural and Fisheries Research and Training (IFAPA), Centro Alameda del Obispo, Alameda del Obispo, 14004 Córdoba, Spain
[3] Department of Biosciences, Biotechnologies and Biopharmaceutics, Faculty of Veterinary Sciences, University of Bari 'Aldo Moro', 70125 Bari, Italy
[*] Correspondence: franciscoj.navas@juntadeandalucia.es; Tel.: +34-638-535-046 (ext. 621262)

Abstract: This study evaluates a method to accurately, repeatably, and reliably extract camel zoometric data (linear and tridimensional) from 2D digital images. Thirty zoometric measures, including linear and tridimensional (perimeters and girths) variables, were collected on-field with a non-elastic measuring tape. A scaled reference was used to extract measurement from images. For girths and perimeters, semimajor and semiminor axes were mathematically estimated with the function of the perimeter of an ellipse. On-field measurements' direct translation was determined when Cronbach's alpha ($C\alpha$) > 0.600 was met (first round). If not, Bayesian regression corrections were applied using live body weight and the particular digital zoometric measurement as regressors (except for foot perimeter) (second round). Last, if a certain zoometric trait still did not meet such a criterion, its natural logarithm was added (third round). Acceptable method translation consistency was reached for all the measurements after three correction rounds ($C\alpha$ = 0.654 to 0.997, $p < 0.0001$). Afterwards, Bayesian regression corrected equations were issued. This research helps to evaluate individual conformation in a reliable contactless manner through the extraction of linear and tridimensional measures from images in dromedary camels. This is the first study to develop and correct the routinely ignored evaluation of tridimensional zoometrics from digital images in animals.

Keywords: endangered breed; perimeters and circumferences; on-field measurements; mathematical modelling; software-assisted image analysis

MSC: 62H35

1. Introduction

Zoometry, or the measurement and comparison of the sizes and proportions of animals or animal parts, has traditionally been considered a key element for breed characterization [1]. Such a determinant role not only relies on the implication of body conformation and dimensions in the definition of breed standards, but also on the functional classification of individuals depending on their better suitability for the development of certain tasks [2]. In these regards, zoometric analysis may help to detect differences among livestock populations or breeds which may be the source for niche specialization or exploration opportunities. As a direct consequence, zoometrics has been reported as one of the driving agents for the conservation (seeking a particular breed standard) and selection strategies (intraherd and interherd breeding criteria definition) that are eventually implemented [3] in local breeds.

Animal body measurements have been traditionally obtained manually with the use of a diverse range of instruments [4]. However, these tasks are not exempt of risks and inconveniences for both the animals and the workers, such as the increased stress induced in the animals or the errors in measurements due to the difficulty of maintaining the animals in a complete stationary position, among others. If sedation or the use of anesthetics is required for animal immobilization due to temperament issues, therefore becoming potentially hazardous to the operators, not only can the animal welfare be compromised, but this also makes the time and costs of the zoometric tasks increase [5].

For these reasons, several methods aiming at automatizing zoometric measurements collection in non-invasive, contactless, cheaper, and faster ways have been attempted in different species over the past decade [6]. Literature has reported the success of bidimensional and tridimensional image-based zoometric analysis methods in domestic and wild animal populations [7–20]. Among them, software-assisted digital imaging zoometrics offers a sound and solid alternative, which has not only solved the aforementioned issues, but also overcome the accuracy of traditional zoometric practices [5,6]. The evaluation of static images may reduce the biases derived from human data collection due to the animals' spontaneous movements. However, the use of high-resolution images may be needed, and inferring certain tridimensional measurements such as perimeters from bidimensional photographs is still critical. In this sense, mathematic modelling can help correct potential computational biases from both linear and tridimensional measures, while at the same time providing an economically affordable opportunity to perform zoometric comprehensive analyses, and the stress induced in animals at the time of being held and measured is substantially minimized [5].

Some minor species such as camels, despite being increasingly prevalent at livestock scenarios for their contemporary recognition as a sustainable species [21], have only anecdotally been attempted for zoometric evaluation and breed characterization [3]. Dromedaries or one-humped camels (*Camelus dromedarius*) are a typical element in the scene of developing economies and constitute the vast majority of the world's camel census. Due to the economical context in which they are normally evaluated and the lack of attention paid to them in the past [21], the scarce initiatives towards morphometrics phenotypic variability collection have mainly been implemented via on-field sampling [1,22–25]. However, these practices are not free from challenges. Indeed, the combination of camels' large size and often strong temper may compromise the integrity of operators [3] and turn zoometric analysis into a dangerous time and a demanding human resources practice [16]. As a consequence, certain measurements, or medial regions like udders [26] and genitals [27], are routinely almost never registered due to the difficulty or danger that their access implies.

Contextually, for the safe accomplishment of on-field zoometric collection, camels need to be properly restrained for their secure handling [4], and the use of a wide diversity of measuring tools is compulsory. Hence, camels still lack contactless methods which may help to safely improve the efficiency and accuracy of zoometrics for camel breed characterization and the definition of adapted selection criteria for the maintenance of camel global genetic diversity [28]. This becomes even more crucial when the camel breed being considered is at risk of extinction and has a very defined applicability for tourism, work development, or therapeutic kinetics [29], as occurs for the Canarian camel.

The early development of image-analysis methodologies for measuring zoometrics in dromedaries is evidenced by the first body zoometric digital reconstruction [30]. As a result, the 3D modeling method is confirmed to be used as a remote method to extract morphological features of camels in a reliable manner. However, the experimental nature of this initiative and the time and costs needed for it to be implemented at a large scale make it compulsory to explore other alternatives. In this sense, a recent investigation has approached the accuracy of image analysis for the extraction of some linear zoometric measurements in dromedaries [31]. Nevertheless, the evaluation of tridimensional measurements (such as perimeters) is still misconsidered. Thus, the relatively scarce data that

are obtained continue to be incomplete, given that relevant functionally important traits might not be recorded [32]. In this framework, the present research aims to develop a standardized and validated method for the comprehensive collection of both linear and tridimensional zoometric measurements in live dromedary camels by using 2D images. The combination of bidimensional digital imaging and logarithmically adjusted Bayesian regression methods provides a timely response to the need for the accurate registration of linear and tridimensional zoometric measurements. The method proposed not only offers a time and money affordable precise alternative that can be used as the main source for breed characterization and functional evaluation at a large scale, but also in a comparative manner which may be translatable to other camel populations.

2. Materials and Methods

2.1. Zoometric Parameter Definition

The bibliography on the topic was reviewed to obtain a comprehensive database of zoometric measurements in camels during the whole month of September 2019. Bibliographic analysis was performed using Google Scholar search engine (https://scholar.google.com/) (accessed on 1 September 2019), as suggested by other papers in which document library data extraction has been performed, due to the possibilities this search engine offers in regards to data extraction [21]. After this document search, six papers dealing with camel zoometrics, regardless of the measuring method used, published from 1994 to 2019, were found [33]. The list of measurements included in the aforementioned documents was completed with other variables relevant for camel functional development [3]. After a variable list was completed, a total of 30 zoometric measures were determined to be collected on-field and later extracted from digital images. Table 1 presents a description of the aforementioned zoometric variables.

Table 1. Description of the zoometric measures in Canarian camels collected for the study.

Area	Measurements	Description
Head	Head length	Distance from the anterior edge of the nasal bones to the nuchal crest.
	Head width	Distance between the midpoint of both orbits.
	Ear length	Distance from the base to the tip of the ear.
	Ear width	Widest distance perpendicular to ear length.
Neck	Neck length: dorsal line	Distance from the base of the neck (cervicothoracic junction) to the base of the head (atlanto-occipital joint) following the upper line of the neck.
	Neck length: ventral line	Distance from the base of the neck (cervicothoracic junction) to the base of the head (jaw angle) following the lower line of the neck.
	Neck girth: cranial third	Circular perimeter of the neck measured at its insertion to the base of the head.
	Neck girth: middle third	Circular perimeter of the neck measured at its middle part.
	Neck girth: caudal third	Circular perimeter of the neck measured at its insertion to the chest.
Thorax and Dorsum	Chest width	Distance between the medial point of the front of the forelimbs, measured at the base of their insertion into the torso.
	Heart girth	Circular perimeter of the chest measured directly behind the sternal callosity and before the hump.
	Height at withers (stature)	Distance from the withers to the ground.
	Body length	Distance between the shoulder to the point of the hip.
	Hump-to-tail distance	Distance between the most caudal point of the base of the hump to the base of the tail.
Hump	Hump length	Distance between the front and the back of the hump passing through the top of it.
	Hump width	Distance between the front and the back of the hump passing through one of its laterals.

Rump and Tail	Hump height	Distance between the middle points of the base of the hump at each lateral, passing through the top of the hump.
	Hump girth	Circular perimeter of the hump measured at its base
	Rump length	Distance from the coxal to the ischial tuberosity.
	Rump width	Distance between the right and left coxal tuberosity.
	Tail length	Distance from the base to the tip of the tail, excluding the tail skirt.
	Width at the base of the tail	Distance between the most lateral points of the base of the tail.
Extremities	Thigh perimeter	Circular perimeter of the thigh measured at its middle part.
	Hock perimeter	Circular perimeter of the hock measured at its middle part.
	Fore cannon bone perimeter	Circular perimeter of the front cannon bone measured at its middle part.
	Rear cannon bone perimeter	Circular perimeter of the hind cannon bone measured at its middle part.
Feet	Sole length	Distance from the front to the back of the sole, measured at the planter surface.
	Length of toe dorsal line	Distance from the external reference of the fetlock to the upper edge of the hoof.
	Heel height	Distance from the caudal point of the fetlock to the ground.
	Foot perimeter	Circular perimeter of the foot measured at its plantar edge.

2.2. Animal Sample

Zoometric record collection took place between September 2019 and August 2020 for 130 Canarian camel breed individuals (58 females and 72 males). Camels were located in three representative emplacements where Canary camels are bred: (Doñana National Park) Huelva (36.972330, −6.427498), Almería (36.902180, −2.429520), and Fuerteventura (28.186777, −14.158361) in Spain. Animals were clinically exanimated to ensure the proper condition of the animals, which enabled their participation in the study. Furthermore, to prevent bias issues derived from the sexual status of the animals at the moment of sampling, sexually immature individuals were discarded (below 3 years of age). Parallelly, only non-gravid she-camels were included in this study, since pregnancy may be a source of bias in zoometric measurements in the thoracoabdominal region [34]. Age or live weight did not normally distribute ($p < 0.05$). Live weight was calculated using the following formula (Equation (1)) by Boujenane [35].

$$\text{Live Weight} = 6.46 \times 10^{-7} (\text{HW} + \text{ChG} + \text{HG})^{3.17} \tag{1}$$

where HW is height at the withers, ChG is chest girth, and hg is hump girth, respectively. The sampling of each of the 30 zoometric measures taken from each animal was collected from its left side following the premises in Iglesias et al. [33] and Alhajeri et al. [3]. Females and males' age and live body weight descriptive statistics are represented in Figure 1.
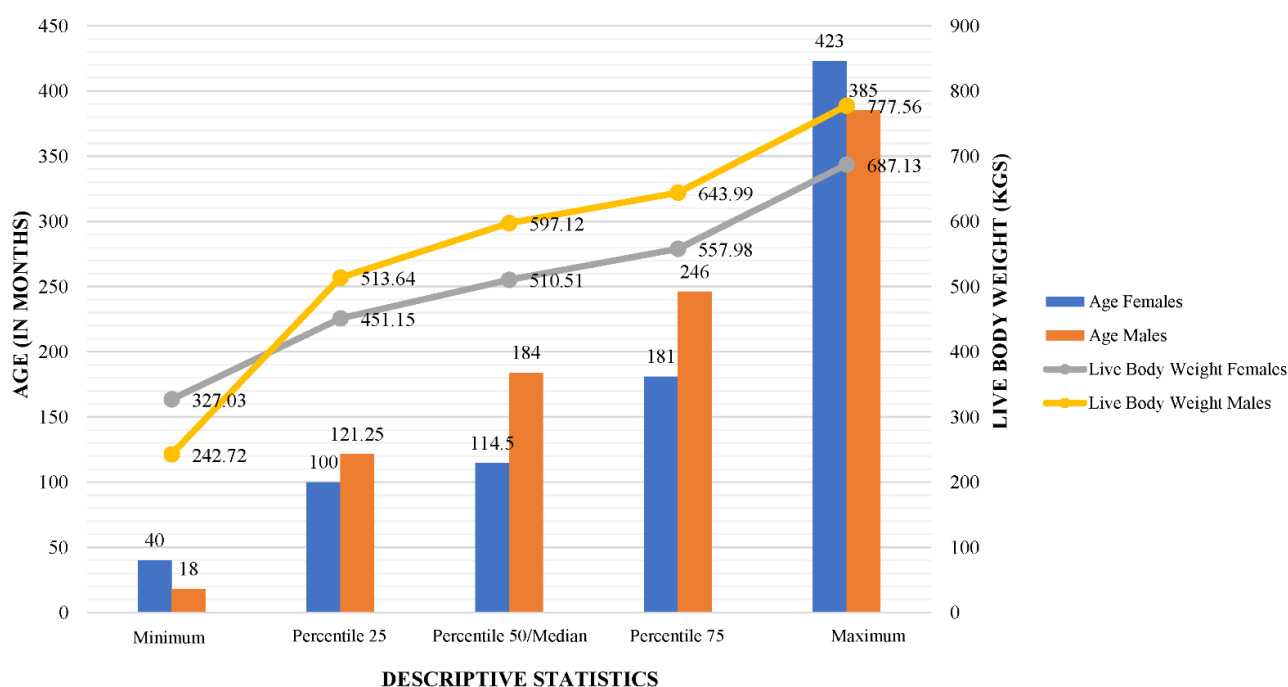
Figure 1. Descriptive statistics for age and live body weight in females and males, respectively.

2.3. Sampling

The end of the molting season, which is a six-to-eight-week period starting in late spring [36], was chosen as the sampling moment to prevent the bias which may potentially be ascribed to hair length and texture [8]. Figure 2 presents a flowchart summarizing the research methodology.
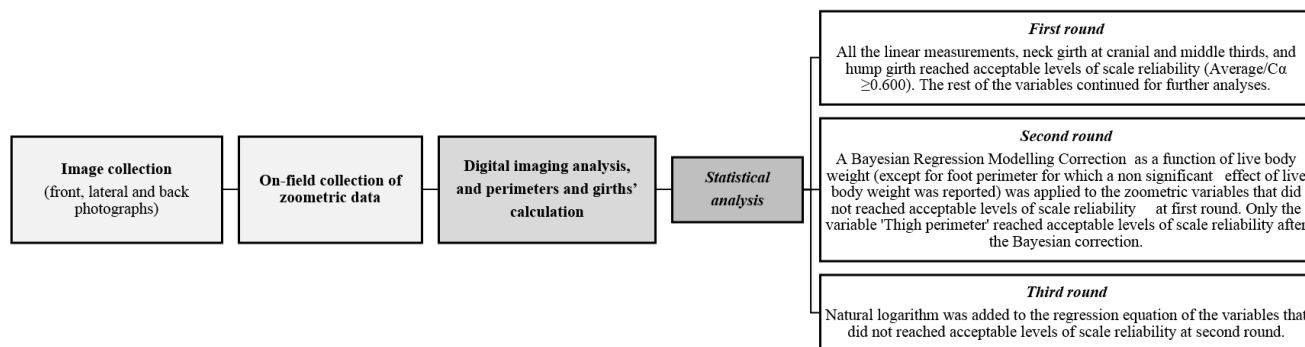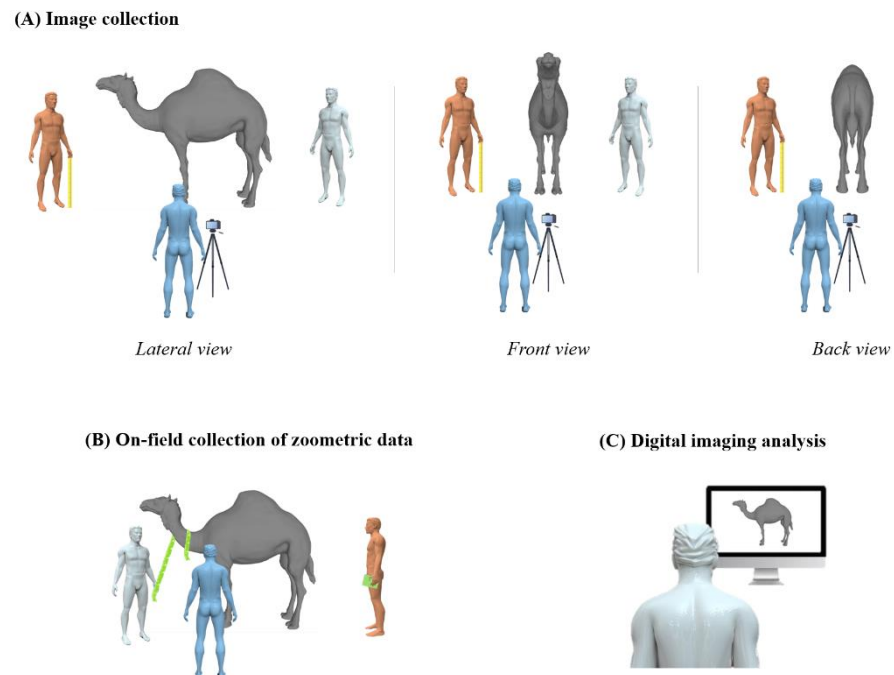

Figure 2. Flowchart summarizing the methodology proposed in the present study.

2.3.1. On-Field Zoometrics

Live animal-based measurements sampling took place with the animals holding a static upright position with their head naturally raised and in correct aplomb (parallel fore and hind legs perpendicular to the ground with lined toes). Animals were measured on a flat and hard ground surface. Measure collection was performed using a non-elastic measuring tape. All operators were trained. The first operator performed on-field measurement collection and digital image measurement extraction. The first operator was assisted by a second operator in zoometric measurements collection, while a third operator annotated the outputs of zoometric evaluation and held a one-meter measuring bar to be used as a reference for calibration on digital zoometrics extraction (Figure 3).

(A) Image collection

Lateral view *Front view* *Back view*

(B) On-field collection of zoometric data **(C) Digital imaging analysis**

Figure 3. Graphic representation of the relative position of operators during across data collection phases. During (**A**) image collection, first operator (Grey) was responsible to hold camel on correct aplomb at a completely static position while keeping the photographic and camel midsagittal planes parallel; second operator was responsible to take photographs for digital imaging analysis; Second operator (Blue): responsible to take photographs for digital imaging analysis, and third operator (Orange): responsible to hold a one-meter measuring bar (yellow bar) near the animal body to be used as a reference for image calibration on digital zoometrics. During (**B**) on-field collection of zoometric data, first (Grey) and second (Blue) operators perform on-field measurement collection with a non-elastic tape (green tape) while third operator (Orange) annotates the outputs of zoometric evaluation. During (**C**) digital imaging analysis, first operator (Grey) performs digital image measurement extraction.

2.3.2. Digital Imaging

Three photographs (front, lateral, and back perpendicular to the camera) were taken per animal right before on-field zoometric evaluation. The second operator took these three photographs for digital imaging analysis (front, lateral, and back views). The third operator was in charge of holding a one-meter measuring bar at the same midline of the body to be used for reference calibration of distances on the computer measurement software for digital imaging zoometrics while taking the aforementioned photographs. The obtained images were digitally processed using Kinovea 0.95 (Free Software Foundation, Inc., Boston, MA). Zoometric linear measurements were obtained in pixels by drawing a straight line between two points in the picture and automatically converted into cm after calibration of the software using the measuring bar as a reference using the *Calibrate* option of the *Line* tool of the software [37]. Puig-Diví et al. [38] reported Kinovea software to be a valid and reliable tool which is able to measure accurately at distances up to 5 m from the object and at an angle range of 90°–45°.

Image collection was performed on an open hard ground and flat area. Light conditions were chosen so as for the animal not to be placed in a shaded area or in one in which light exposure may distort image capture. The animal color was considered to ensure background color did not lead to any measure distortion or measure misregistration. The camera was positioned at a standardized height of 1 m on a camera stand 4 m away from the camel center of balance. The aforementioned distance and height permitted framing

of the animals being evaluated on the whole. We followed the premises in Iglesias et al. [33] to determine the proper aplomb of the animals and tracing standard lines on the ground before photograph taking to ascertain the animal was in the right position. Image capture was performed using a digital camera (Sony DSC-RX100 SENSOR CMOS Exmor 1.0 of 20.1 MP, F1.8-4.9, Zoom 20-100, Optical Zoom 3.6×, 3" LCD Screen Image stabilizer) in standard mode. Joint Photographic Experts Group (JPEG) compression format was used. One trained operator performed zoometric measurement digital extraction from photographs manually.

2.4. Statistical Analysis

2.4.1. Method Comparison/Reproducibility and Repeatability: Interobserver Correlation Coefficient (ICC)

Intraclass correlation coefficient (ICC), based on multiple paired Cohen's κ tests, was run to compare zoometric on-field analysis to digital imaging zoometric analysis. As suggested in Bunting et al. [39], the intraclass correlation coefficient (ICC) is a reference method to determine the reproducibility and reliability of numeric measurements organized into groups beyond a simple pairing, for example, different operators measuring the same variable in different animals or the same operator using different methods on different animals. In this study, we issued the equations, and equations were solved. Then, we used ICC to compare the results from model solving and real measurements to test for the reproducibility and reliability of models.

Fleiss and Cohen [40] established reproducibility/repeatability guidelines for ICC interpretation as less than 0.4 (low); between 0.4 and 0.59 (reasonable); 0.6 to 0.74 (good); and 0.75 to 1.0 (excellent) to determine whether reproducible, repeatable, and reliable enough levels were attained. A "Two-Way Random" model was chosen from the premises in Koo and Li [41]. Then, we computed 95% confidence intervals after the following expression 95% kappa Confidence Interval (95%CI) = κ ± 1.96 SEκ, where SEκ = ((po (1 − po)/n (1 − pe) 2) 0.5, with the reliability analysis routine of the scale procedure of SPSS Statistics for Windows, Version 25.0, IBM Corp. (2017).

2.4.2. Scale Reliability and Repeatability: Cronbach's Alpha (Cα)

Instrument scale internal consistency was measured using Cα. Internal consistency, when applied to instrument comparison, is an estimate of 'reliability based on the average correlation among items within a test', with each of these items being each of the measuring methods, zoometric on-field evaluation, and zoometric digital imaging, in our case [42], and examines the degree to which such instruments measure the same characteristics or domains of knowledge [43]. Typically, internal consistency is measured by the calculation of a reliability coefficient [43], such as Cα.

In this context, Cα represents the reliability level of the instrument being compared to a reference instrument (zoometric digital imaging to zoometric on-field analysis as a reference) [44]. As a general criterion, George and Mallery [45] suggest the following recommendations for evaluating Cα coefficients: >0.9 is excellent, >0.8 is good, >0.7 is acceptable, >0.6 is questionable, >0.5 is poor, and < 0.5 is unacceptable. However, when comparing internal consistency between instruments, Pallant [46] reported that Cα value above 0.6 is considered a highly reliable and acceptable index [42]. Furthermore, retaining variables with values over 0.5 has been suggested due to their ability to explain data variability [47].

As suggested by González Ariza et al. [47], single measures of ICC determine how a single observation taken at random may correlate to another single observation, that is, in our case, how a zoometric measure from on-field evaluation may correlate with its paired counterpart from digital imaging. By contrast, average ICC and Cα determine how consistent the set of instruments being compared are on average. Consequently, in instrument comparison, average measures somehow prevent potential measuring errors affecting

particular measurements, and as a result, report erroneously decreased instrument reliability and accuracy values for the instrument being tested (digital imaging zoometrics in our case).

### 2.4.3. Parametric Assumptions Testing and Approach Decision

The statistical approach was decided after parametric assumptions testing. The Shapiro–Francia W' test (for 50 < n < 2500 samples), Shapiro–Wilk test (for n < 50 samples), and Levene's test were used to determine whether normality and homoscedasticity parametric assumptions were met. The Shapiro–Francia W' test was run using the Shapiro–Francia normality routine of the test and distribution graphics package of the Stata Version 15.0 software (StataCorp, College Station, TX, USA) [48]. Homoscedasticity was run using the explore procedure of the descriptive statistics package in SPSS Statistics (Version 25.0, IBM Corp., Armonk, NY, USA) [49].

2.4.4. Perimeters and Girths Calculation

As suggested by Singaraju et al. [50] in their study performing ellipsoid biometric computations, Ramanujan's equation of ellipse model for ellipsoid perimeter (P) was used to fit zoometric perimeters and girths (neck girth (cranial, middle, and caudal thirds), heart girth, hump girth, thigh perimeter, hock perimeter, fore cannon bone perimeter, rear cannon bone perimeter, and foot perimeter, respectively) as follows;

$$P \approx \pi(a + b)\left(1 + \frac{3h}{10 + \sqrt{4 - 3h}}\right) \tag{2}$$

where *a* is the semimajor axis, *b* is the semiminor axis, and h is computed as follows h = ($a - b$)^2/($a + b$)^2. This approximation is within about 5% of the true value, as long as a is not more than three times longer than *b*. Figure 4 schematically represents semimajor and semiminor axis digital imaging collection references for perimeters and girths computation. Ramanujan's equation of the ellipse model was applied using Microsoft Office Excel 2016 as suggested in the literature [51,52].
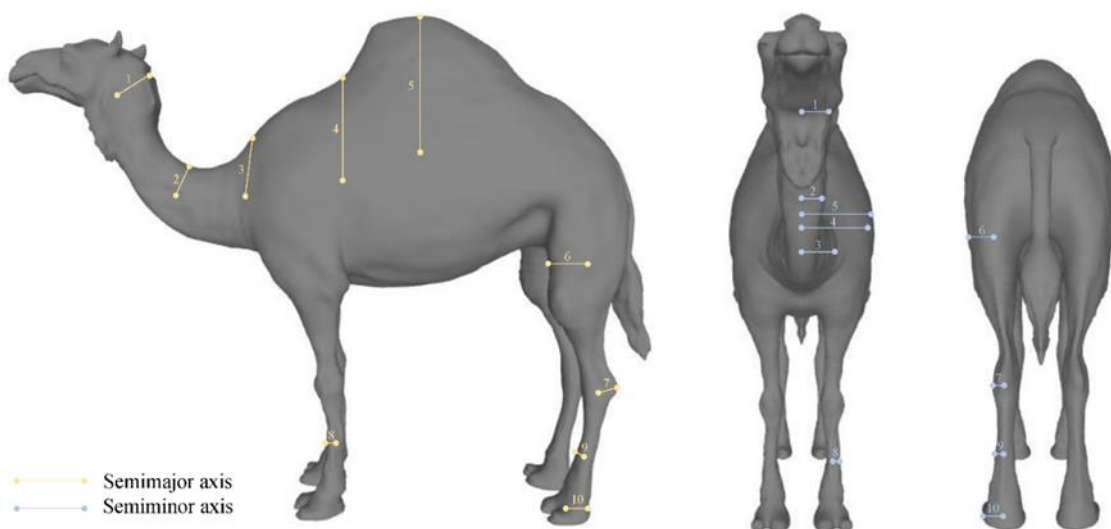
Figure 4. Schematic representation of semimajor and semiminor axis digital imaging collection references for perimeters and girths computation in Canarian camels. (1) Neck girth: cranial third; (2) Neck girth: middle third; (3) Neck girth: caudal third; (4) Heart girth; (5) Hump girth; (6) Thigh perimeter; (7) Hock perimeter; (8) Fore cannon bone perimeter; (9) Rear cannon bone perimeter and (10) Foot perimeter.

2.4.5. Bayesian Linear Regression Modelling and Natural Logarithmic Correction for Perimeters and Girths

Limited sample sizes derived from endangered populations may distort the distribution of variables that are presumably sampled from normally distributed populations, such as zoometrics. Such distortion may be ascribed to highly skewed data appearing as a result of valid outliers. A valid outlier would be an animal that is considerably smaller or larger than the rest, but which may still fit in the context of an endangered breed standard, even if it statistically distorts sample distribution properties.

If valid outliers are not present, skewness may not be forced towards one of the distribution ends, and applying the logarithmic bias correction may not be necessary. However, body score condition and live body weight have been reported to act as sources of bias when performing zoometric analyses in dromedary camels [35]. The bias effect of other factors, such as age or coat color, was also considered.

In such cases, regressing the variable measured in the field against the potentially originating factor of the bias during the collection of measurements from digital sources (live body weight, age, or coat color in our case) and the same variable measured with digital methods (given our aim is to perform a comparison between methods) may have to be performed to ensure the replicability between methods. This ensures that the accuracy of estimation of real measurements after digital measurements is maintained.

The effects derived from outlier distortion become stronger in perimeters, girths, or circumferences calculations given that these cannot be extracted from photographs straight away. The inability to account for such a bias while evaluating tridimensional zoometric parameters from bidimensional images makes it compulsory to apply correction methods. According to the Energy Information Administration of the United States [53], to correct for skewness derived bias in estimations, a bias correction should be issued. To solve this issue, the Energy Information Administration of the United States [53] suggests that sample size limitations could be buffered by regressing the log transformation of the variable to which regression models were initially aimed.

Once the variable measured in the field has been regressed against the potentially originating factors of the bias, and the same variable is measured with digital methods, bias correction may be obtained after summing the outcomes of this regression to the natural logarithm of the zoometric variable measured using digital methods.

In these contexts, the application of regression equations may be difficult due to the alteration of sample properties and ordinary least squares regression assumptions. However, these distribution distortions events may be saved using statistical alternative methods such as Bayesian linear regression, which are less sensitive to outliers and distribution alterations [54], and their estimations may be subject to wide confidence intervals.

Valid outliers' detection in our data sample was performed using the *identify outliers* procedure of the *Analyze/Built-in* analysis of the column analyses package of GraphPad Prism version 8.3.0. The ROUT method was applied to prevent the effects of outliers. The ROUT method combines robust regression and outlier removal and is based on the false discovery rate (FDR). A maximum desired FDR must be predefined (Q coefficient). ROUT method assumes all data except for outliers to be sampled from a Gaussian distribution. When data does not meet the aforementioned assumption, outliers may follow the same distribution as data.

The ROUT method strength to detect outliers was determined using the Q coefficient. Higher levels of Q are indicative of lower threshold strictness for outliers' detection, thus, the higher the outlier detection power, but also the higher the probability for a false outlier to be identified as a true one. Lower Q values set stricter thresholds for outlier definition, which consequently translates into lower power to detect real outliers, but also lower chances for false outlier consideration. A Q coefficient of 1% is the recommended threshold to be used as a default [55], given it implies a lower than 1% false discovery rate for outlier detection.

Consequently, after considering the presence of outliers, when evidence of a lack of acceptable fit ($C\alpha$ < 0.600) between perimeter or girth on-field zoometric evaluation and digital imaging mathematical computation using Ramanujan's equation for ellipsoid perimeter was found, we used Bayesian linear regression modelling to correct measurement as a function of live body weight.

The presumably large dependence of zoometric parameters on age may have suggested the inclusion of age in the regression models, as according to Carlin [56], Bayesian inferences are sensitive to the dependence of variables on time (conditional on θ and x). In our case, zoometric analyses were performed when animals had reached the adult stage to prevent age-derived biases from occurring, as suggested by the lack of pieces of evidence or a significant effect of age (p > 0.05). Contextually, the age variation coefficient (CV) was 0.598. As a rule of thumb, a CV ≥ 1 indicates a relatively high variation, while a CV < 1 can be considered low, hence, the lack of a significant interindividual variability prevented age from being considered as a covariate.

Pieces of evidence for a non-significant bias effect of coat color effect were also reported (p > 0.05 and CV of 0.376). This lack of bias ascribed to coat color variability may derive from the fact that photographs were taken once the hair molting season had passed and an appropriate lighting scenario that remarked the topographic shadows of bone accidents (references for measurement) had been considered. Furthermore, animals were photographed and measured by the same people trained for this purpose, with the same technological equipment, and information regarding their coat color was registered to minimize the effects of the aforementioned potentially biasing factors.

Those zoometric perimeters and girths did not reach acceptable levels of scale reliability ($C\alpha$ < 0.600), and hence were considered the dependent variables of Bayesian regression models to apply body live weight correction.

As suggested in Koehrsen [57], Bayesian linear regression uses probability distributions rather than point estimates. This means response, y, is not estimated as a single value, but is assumed to be drawn from a probability distribution. The output, y, is generated from a normal (Gaussian) distribution characterized by a mean (the transpose of the weight matrix multiplied by the predictor matrix) and variance (the square of the standard deviation σ, multiplied by the identity matrix, given it is a multi-dimensional model formulation). Hyperparameters' means and variance were used to obtain the best values of the hyperparameters of the prior distribution, as suggested by Kundu [58].

The objective of Bayesian linear regression is to determine the posterior distribution for the model parameters, rather than the best value for model parameters. Not only is the response generated from a probability distribution, but the model parameters presumably come from the same distribution. The posterior probability of the model parameters is conditional on the training inputs and outputs. In contrast to frequentist Ordinary Least Squares Regression (OLS), there is a posterior distribution for the model parameters proportional to the likelihood of the data multiplied by the prior probability of the parameters.

This implies two primary benefits of Bayesian linear regression: priors and posteriors. When there is knowledge, or a guess for what the model parameters should be, these priors can be included in the model (for example, the influence of live body weight on zoometrics). This approach contrasts the frequentist approach, which assumes everything there is to know about the parameters comes from the data. Indeed, in Bayesian regression, when there is no prior information known, non-informative priors for the parameters such as a normal distribution can be used.

Afterwards, posteriors, or the results of performing Bayesian linear regression, are a distribution of possible model parameters based on the data and the priors. Posteriors enable quantifying uncertainty about the model. Hence, the fewer data points, the greater the dispersion of posterior distribution will be. As the amount of data points increases, the likelihood washes out the prior, and in the case of infinite data, the outputs for the parameters converge to the values obtained from OLS.

To summarize, in Bayesian inference for linear regression, we use priors as initial estimates, and as we gather more evidence, testing our model against data (posteriors), the model supports or disproves our prior hypotheses. In practice, the evaluation of the posterior distribution for the model parameters is intractable for continuous variables when we implement Bayesian linear regression. Thus, sampling methods are used to draw random samples from the posterior distribution to approximate the posterior distribution to which it should be using Monte Carlo algorithms method and its variants.

The (Metropolis–Hastings) random walk algorithm, which uses Markov Chains to perform Monte Carlo estimate via the Gibbs Sampler algorithm, was used as aforementioned given a different prior to the default uniform prior specified in IBM SPSS Statistics Algorithms v. 25.0. by IBM Corp. [59] was selected. The random walk Metropolis algorithm is the preferable option for data imputation from the collection of Markov Chain Mote Carlo (MCMC), as suggested in MacKay [60], given that neither admissibility nor stability were selected.

The following general equation was used for each of the regression models defined in this study $y_i = X_1\beta_1 + \dots X_i\beta_i + \varepsilon_i$, where $i = 1, 2, \dots i$ is the ith number of factors; y_i is the vector of records for the aforementioned dependent variables with dimension n (a total of 910 records, one record per each of the seven circumferences/perimeters which did not reach acceptable reliability levels and each of the 130 dromedary camels measured); X_i is the appropriate incidence matrix for factors; β_i is the standardized regression coefficients for the ith number of factors and covariates considered, respectively. The general regression equation used for each perimeter or girth was Y = Intercept + $\beta_\text{on field perimeter/girth (cm)}$·on-field perimeter/girth (cm) + $\beta_\text{Live body weight (Kg)}$·body live weight (Kg).

As Brewer [61] suggested, the intercept was necessary given that we used unstandardized coefficients. The magnitude of intercept confidence intervals was an empirical indicator of the need for its estimation. Residual effects (ε_i) normality was assumed as follows $\varepsilon_i | X_i N(0, \sigma_{\varepsilon i}^2)$, where $X_{\varepsilon i}$ is an identity matrix and $\sigma_{\varepsilon i}^2$ is the residual variance, respectively. Continuous predictor variable unstandardized coefficients were produced by the linear regression model using the independent variables measured in their original scales.

As suggested by Hayes et al. [62], unstandardized coefficients (βi) can be defined as the average increase of βi units in Y associated with an increase of one unit in $X i$ maintaining the rest of the variables constant. Below, a detailed summary of the priors and posterior distributions used in this study is reported. The complete description of the algorithms used by SPSS to perform Bayesian inference on multiple linear regression models in this study can be found in IBM SPSS Statistics Algorithms v. 25.0. by IBM Corp. [59].

Quadratic approximation was discarded (even if it has been reported to be computationally faster in terms of discretization and computing the likelihood over all possible parameter combinations). Instead, the Markov Chain Monte Carlo (MCMC) approximation was used, as it does not assume the fact that the posterior distribution follows a normal distribution.

Bayesian linear regression analyses were performed using the linear regression package from the Bayesian statistics task of SPSS Statistics, Version 25.0, IBM Corp. [49]. The Bayesian linear regression test routine of the linear regression and related package of the Stata Version 16.0 software process was used to compute posterior distribution statistics for the factors considered. Afterwards, we evaluated the estimated effect of the factors considered in the resulting predictive models, its confidence intervals, and posterior distribution statistics to build linear regression equations, calculate digital perimeter/girth extrapolation, and ICC was run again. When Cα had not significantly improved over acceptable levels, the natural logarithm of each particular perimeter or girth was added to each aforementioned equation, and ICC was calculated again to ensure that reliability levels had been attained.

2.4.6. Jeffrey–Zellner–Siow (JZS) Mixture of g-Priors

The Jeffrey–Zellner–Siow mixture of *g*-priors [63] was used given it successfully satisfies several theoretical requirements such as the equality constraint on the test-relevant parameters, for instance of β, which leads to the null hypothesis $H_0 = \beta = \beta_0$ [64], as suggested by Heck [65]. Rouder et al. [66] and Liang et al. [63] also acknowledged the benefits of JSZ prior distribution. Contextually, conditional on the residual variance ($\sigma_{\varepsilon i}^2$), the JZS prior defines a multivariate Cauchy distribution for the slope parameters of the full model, as follows.

$(\beta_i | \sigma_{\varepsilon i}^2) \sim \mathrm{MVC}(0_P, \gamma_i^2 \sigma_{\varepsilon i}^2 C_i^{-1})$, which is defined by a P-dimensional zero vector (location vector) and a scale matrix. The constant γ_i measures the magnitude of scaling and is a priori chosen by the user, the residual variance $\sigma_{\varepsilon i}^2$, and the matrix $C_i = X_i' X_i / N_i$, which is the covariance matrix of the centred design matrix X_i.

JZS prior [66] is especially appropriate in Bayesian linear regression analyses given that it is symmetric and centered at zero, as explained by Bayarri et al. [67]. This means that positive and negative values of the parameters of the slope are a priori equally likely to occur. Moreover, JZS prior does not depend on the scale of the variables, factors, or covariates considered. Hence, the Bayes factor is scale-invariant, and outputs remain the same when the variables expressed in different units are evaluated, which is likely to occur in multifactorial studies.

Scaling the multivariate Cauchy distribution by the residual variance $\sigma_{\varepsilon i}^2$ ensures the achievement of such independence from the measurements of model elements (a priori, a larger residual variance implies larger slopes) and by the inverse of the covariance matrix C_i (a priori, a covariate with a larger variance implies smaller slopes). In this context, the process of definition of scaled priors for unstandardized coefficients (β_i) equals the process of definition of priors for standardized coefficients (β_i^*) [66].

Third, the scale parameter γ is fixed to a constant, hence prior beliefs are specified about the expected effect size remain constant as well. The IBM Corp. [59] algorithm guide, in its section for the algorithm of JZS prior for linear regression analyses, sets the default value of $\gamma = 2\sqrt{\pi} = 3.5$ to compute Bayes Factor. This reflects a belief of a priori medium effect size, which, for a single covariate x, implies a priori probability for the standardized regression slope $\beta_i^* = \beta_i \cdot \mathrm{SD}(x_i)/\sigma_i$ of 53.2% of being in the range (−0.50, +0.50).

Rouder and Morey [68] explained other benefits from the choice of the JZS prior, for instance, its model selection aimed at consistency (this is that Bayes factor, goes to infinity as the number of observations N increases without bound-favoring the data-generating model) or consistency in information (the Bayes factor for a certain effect goes to infinity as the proportion of explained variance or R Squared (R^2) increases to 1). Additionally, Bayes factors for JZS prior are highly precise and relatively easy to compute [69], resulting in its wide applicability for the default *t*-test [70], ANOVA [66], and linear regression [65].

2.4.7. Bayesian Modelling of Factor and Covariate Effects (FCEBM)

Being y_i, any of the effects of any of the independent variables (covariates) considered in this study (live body weight, age, and coat color), the posterior distribution of y_i in the context of the data, D, is

$$p(y_i / D) = \sum_{i=20}^{i} p(y_i | M_i, D)\, p(M_i | D) \qquad (3)$$

This means each model's average of posterior distributions is weighted by their posterior model probabilities. In the aforenoted equation, the posterior predictive distribution of y_i given a particular model M_i is,

$$p(y_i | M_i D) = \int p(y_i | \beta_i, M_i, D) p(\beta_i | M_i D)\, d\beta_i \qquad (4)$$

and the posterior probability of the model M_i is given by

$$p(M_i|D) \; = \; \frac{p(D|M_i)p(M_i)}{\sum_{i\,=\,20}^{i} p(D|M_i)p(M_i)} \qquad (5)$$

where,

$$p(M_i|D) \; = \; \int p(D|\beta_i, M_i)p(\beta_i|M_i) \, d\beta_i \qquad (6)$$

is the integrated probability of the model M_i, β_i is the vector of parameters of the model M_i, $p(\beta_i|M_i)$ is the prior density of β_i under model M_i, $p(D|\beta_i|M_i)$ is the probability, and $p(M_i)$ is the prior likelihood that M_i is the true model.

The number of models (K) for a problem with P potential covariates can be enormous (K = 2^P in the absence of other constraints). Only a small number of these K models will be sufficiently supported by the data, and hence selected by SPSS for each of the P covariates. Gibbs sampling algorithm was used to estimate marginal posterior distributions of all unknowns.

2.4.8. Factors and Covariate Effect Bayesian Interpretation (CEBI)

The detection of issues before model estimation was evaluated using the checklist proposed by Depaoli and Van de Schoot [71]. Among the issues checked, we tested for those occurring after model estimation before interpreting results, in priors' influence comprehension, and after interpreting results for conclusion drawing. Interpreting the effect of each particular covariate (independent variables used in this study) was made as follows.

First, the posterior probability $p[\beta_i^* \neq 0/D]$ expresses the probability that every single independent factor or covariate affects each particular dependent variable. Standard rules of thumb [72] for posterior probability interpretation are as follows: <50% evidence against the effect; 50–75% weak evidence; 75–95% positive evidence; 95–99% strong evidence; >99% very strong evidence, which is comparable to commonly used thresholds that define the level of significance of evidence using Bayes factor (BF) (Supplementary Table S1).

Second, posterior distribution means determines the magnitude of the effect of every single factor and covariate. For metric covariates (continuous predictors) or the numeric variables used in this study, regression coefficients define the difference in the predicted value of the response variable for each one-unit change in the predictor variable, with all other predictors being constant. When dependent variables are metric, β regression coefficients are a measure of effect sizes by themselves.

Third, a 95% credibility interval suggests that a 95% likelihood for these regression coefficients (every single covariate and factor posterior distribution means) lies within the corresponding credibility intervals. A significant effect is reported when 0 is not contained within the credibility interval for each particular factor. In the present study, only live body weight significantly influenced zoometric measurements ($p < 0.05$).

2.4.9. Convergence Criterion

Iteration rounds continued until a tolerance convergence criterion of 10^{-8} was reached [73]. After this, initial parameters were defined, and model fitting properties were analyzed. The maximum number of iteration rounds was 2000 for each analysis as stated in IBM SPSS Statistics Algorithms version 25.0 by IBM Corp. [59]. Such a convergence criterion was defined given its wide application in Bayesian ANOVA and linear regression analyses in limited sample sizes research contexts [74].

2.4.10. Model Validity and Explanatory Power of Present Data, and Predictive Power of Future Data

Validation and comparison of Bayesian models were described in Geweke [75]. Contextually, other authors [76] suggest model validation should base on models' mean square error (MSE). Although mean square residual or error (MSE) and minimum mean-

square residual or error (MMSE) have been widely used to measure the closeness between a regression line and a set of points (model fit to explain data), mean square prediction error, or MSPE (=RSS/no. of observations), was used to measure error variation due to the MSE being influenced by the number of predictors [77] in reduced sample sizes cases [78,79].

The residual sum of squares (RSS) quantifies the amount of variability in a data set not explained by a regression model. That is, the RSS measures the amount of error remaining between the regression function and the data set, thus it essentially defines the ability of a certain regression model to explain or represent the data. Smaller values of RSS are indicative of better suitability of the regression function to model for the data it intends to model.

Specific to Bayesian inference, Monte Carlo standard error (MCSE), which is defined as the standard deviation of the chains divided by their effective sample size, measures the accuracy of the chains. MCSE is the non-parametric or Bayesian counterpart of MSPE, and should be used as the validation criteria in Bayesian linear regression model comparison studies [80].

Bayes factor (BF) is an indirect measure of models' explanatory power to describe observed data. Larger values of BFs evidence higher probabilities for the combinations of the factors modelled to explain dependent variables. Supplementary Table S1 reports common thresholds to define the significance of evidence as suggested by Jeffreys [81] and Lee and Wagenmakers [82]. Bayesian R^2 is related to BF and can be considered as a data-based estimate of the fraction of variance explained for data. Parallelly, acceptance rate, efficiency, and Monte Carlo standard error (MCSE) were used to determine Bayesian methods' validity. Supplementary Table S2 presents the description and interpretation of model validity parameters. The predictive accuracy of the model's Bayesian statistics [83] can be estimated through posterior predictive checking [84].

Afterward, the Bayesian information criterion (BIC) or Schwarz information criterion (also SIC, SBC, SBIC) was calculated to determine the model predictive ability of new data as follows:

$$BIC \;=\; N * N \ln(MCSE) + K * \ln(N) \tag{7}$$

where MCSE is the Monte Carlo standard error, N is the number of observations or records, and K is the number of independent parameters of the model.

BIC was used to compare predictive power across models as it considers the statistical goodness of fit and the number of parameters to be compulsorily estimated to reach such fitness degree, as it penalizes every time the number of parameters considered increases [85,86]. As a result, BIC quantifies the balance between model fit and model complexity [87]. Lower BIC values mean that a particular model is a comparatively better predictive model than the rest. Contrastingly, Bayesian R^2 estimates the explanatory power of observed data.

In consequence, although the addition of "noise" variables to the fit, variables that explain small redundant fractions of variance, will slightly increase R^2 values, model predictive power will decrease (as denoted by its higher BICs). Indeed, as more variables are added to the model, its predictive accuracy decreases. This is, higher R^2 will also translate into higher—and therefore worse—BIC values.

3. Results

3.1. Parametric Assumptions Testing and Approach Decision

All variables did not grossly meet the normality assumption ($p < 0.01$), respectively. Homoscedasticity was violated as well ($p < 0.01$), hence, a parametric approach was discarded, and Bayesian methods resulted in being the most preferable option. No likely outlier was detected, and therefore we preserved all observations for further analyses.

3.2. Initial/First Round of Method Comparison/Repeatability and Scale Reliability

Among the zoometric perimeters and girths measured, neck girth at cranial and middle thirds and hump girth reached acceptable levels of scale reliability (Average/Cα ≥ 0.600, Table 1). Therefore, their direct extrapolation after the application of Ramanujan's equation of the ellipse model for ellipsoid perimeter calculation was feasible and no further analysis was performed. The rest of the variables, which did not reach acceptable reliability levels, continued for further analyses (Average/Cα < 0.600, Table 2).

Table 2. Intraclass correlation coefficient (ICC) for single and average measurements (Cronbach's alpha, Cα) comparison between on-field zoometrics and digital imaging zoometrics.

Area	Measurements	Parameters	Intraclass Correlation	95% Confidence Interval Lower Bound	95% Confidence Interval Higher Bound	F Test with True Value 1	df1	df2	Sig	Round [a]
Head	Head length	Single	0.975	0.965	0.982	78.434	129	129	0.001	
		Average/Cα	0.987	0.982	0.991	78.434	129	129	0.001	1st
	Head width	Single	0.738	0.649	0.808	6.64	129	129	0.001	
		Average/Cα	0.849	0.787	0.894	6.64	129	129	0.001	1st
	Ear length	Single	0.854	0.800	0.895	12.697	129	129	0.001	
		Average/Cα	0.921	0.889	0.944	12.697	129	129	0.001	1st
	Ear width	Single	0.875	0.827	0.910	14.973	129	129	0.001	
		Average/Cα	0.933	0.906	0.953	14.973	129	129	0.001	1st
Neck	Neck length: dorsal line	Single	0.847	0.791	0.890	12.108	129	129	0.001	
		Average/Cα	0.917	0.883	0.942	12.108	129	129	0.001	1st
	Neck length: ventral line	Single	0.992	0.989	0.994	247.029	129	129	0.001	
		Average/Cα	0.996	0.994	0.997	247.029	129	129	0.001	1st
	Neck girth: cranial third	Single	0.556	0.425	0.664	3.504	129	129	0.001	
		Average/Cα	0.715	0.596	0.798	3.504	129	129	0.001	1st
	Neck girth: middle third	Single	0.664	0.555	0.750	4.947	129	129	0.001	
		Average/Cα	0.798	0.714	0.857	4.947	129	129	0.001	1st
	Neck girth: caudal third	Single	0.541	0.407	0.652	3.357	129	129	0.001	
		Average/Cα	0.702	0.579	0.789	3.357	129	129	0.001	3rd
Thorax and Dorsum	Chest width	Single	0.779	0.701	0.838	8.036	129	129	0.001	
		Average/Cα	0.876	0.824	0.912	8.036	129	129	0.001	1st
	Heart girth	Single	0.682	0.578	0.764	5.285	129	129	0.001	
		Average/Cα	0.811	0.732	0.866	5.285	129	129	0.001	3rd
	Height at withers (stature)	Single	0.986	0.979	0.990	152.735	129	129	0.001	
		Average/Cα	0.993	0.989	0.995	152.735	129	129	0.001	1st
	Body length	Single	0.865	0.814	0.902	13.78	129	129	0.001	
		Average/Cα	0.927	0.897	0.949	13.78	129	129	0.001	1st
	Hump-to-tail distance	Single	0.984	0.977	0.989	123.989	129	129	0.001	
		Average/Cα	0.992	0.989	0.994	123.989	129	129	0.001	1st
Hump	Hump length	Single	0.905	0.868	0.932	20.049	129	129	0.001	
		Average/Cα	0.950	0.929	0.965	20.049	129	129	0.001	1st
	Hump width	Single	0.989	0.985	0.992	182.709	129	129	0.001	
		Average/Cα	0.995	0.992	0.996	182.709	129	129	0.001	1st
	Hump height	Single	0.995	0.992	0.996	375.396	129	129	0.001	1st

		Average/Cα	0.997	0.996	0.998	375.396	129	129	0.001	
	Hump girth	Single	0.587	0.461	0.689	3.838	129	129	0.001	
		Average/Cα	0.739	0.632	0.816	3.838	129	129	0.001	1st
	Rump length	Single	0.938	0.914	0.956	31.371	129	129	0.001	
		Average/Cα	0.968	0.955	0.977	31.371	129	129	0.001	1st
Rump and Tail	Rump width	Single	0.984	0.978	0.989	124.652	129	129	0.001	
		Average/Cα	0.992	0.989	0.994	124.652	129	129	0.001	1st
	Tail length	Single	0.984	0.977	0.988	121.041	129	129	0.001	
		Average/Cα	0.992	0.988	0.994	121.041	129	129	0.001	1st
	Width at the base of the tail	Single	0.842	0.783	0.885	11.642	129	129	0.001	
		Average/Cα	0.914	0.879	0.939	11.642	129	129	0.001	1st
	Thigh perimeter	Single	0.618	0.500	0.714	4.239	129	129	0.001	
		Average/Cα	0.764	0.666	0.833	4.239	129	129	0.001	2nd
	Hock perimeter	Single	0.753	0.668	0.819	7.107	129	129	0.001	
Extremities		Average/Cα	0.859	0.801	0.901	7.107	129	129	0.001	3rd
	Fore cannon bone perimeter	Single	0.612	0.492	0.709	4.156	129	129	0.001	
		Average/Cα	0.759	0.660	0.830	4.156	129	129	0.001	3rd
	Rear cannon bone perimeter	Single	0.529	0.393	0.642	3.243	129	129	0.001	
		Average/Cα	0.692	0.564	0.782	3.243	129	129	0.001	3rd
	Sole length	Single	0.718	0.623	0.792	6.097	129	129	0.001	
		Average/Cα	0.836	0.768	0.884	6.097	129	129	0.001	1st
	Length of toe dorsal line	Single	0.894	0.853	0.924	17.832	129	129	0.001	
Feet		Average/Cα	0.944	0.921	0.960	17.832	129	129	0.001	1st
	Heel height	Single	0.977	0.968	0.984	86.753	129	129	0.001	
		Average/Cα	0.988	0.984	0.992	86.753	129	129	0.001	1st
	Foot perimeter	Single	0.486	0.343	0.607	2.894	129	129	0.001	
		Average/Cα	0.654	0.511	0.756	2.894	129	129	0.001	3rd

[a] First: Variables for which direct translation between methods was feasible; Second: Variables for which Bayesian regression modelling correction as a function of digital measurements and live body weight was performed (except for foot perimeter, for which live body weight did not report a significant effect ($p < 0.05$)); Third: Variables for which Bayesian regression modelling correction as a function of live body weight and natural logarithm correction addition was performed.

3.3. Bayesian Linear Regression Modelling and Second Round of Method Comparison/Repeatability and Scale Reliability

After the initial round of method comparison/repeatability and scale reliability, neck girth at caudal third, heart girth, thigh perimeter, hock perimeter, fore cannon bone perimeter, rear cannon bone perimeter, and foot perimeter, respectively, did not reach acceptable levels of scale reliability (Average/Cα < 0.600, Table 2). Hence, we subjected them to Bayesian Regression Modelling Correction as a function of live body weight (except for foot perimeter, for which a nonsignificant effect of live body weight was reported $p < 0.05$), and the second round of ICC computation was performed. We did not consider additional factors such as coat color or age, given no evidence for their significant effect was found ($p > 0.05$). Table 3 summarizes Bayesian unstandardized linear (β) regression coefficients posterior distribution statistics for each of the variables considered. Bayesian determination coefficients (R^2) or percentages of variance captured by each of the models and their

respective BF are provided in Table 4. Models were considerably more probable than those which only comprised the intercept. Posterior predictive *p* values (pppvalues) for models were 0 < pppvalues < 1 and around 0.500, so therefore model fit was ensured (Table 5).

Table 3. Bayesian estimates of posterior distribution statistics for unstandardized linear regression coefficients for digital measurements and live body weight as regressors for the zoometric traits for which Average/Cronbach's alpha did not surpass 0.600 at direct translation in the first round.

Zoometric Trait (=y)	Parameter	Posterior			95% Credible Interval	
		Mode	Mean	Variance	Lower Bound	Upper Bound
Corrected Neck girth: caudal third	Intercept	40.713	40.713	214.839	11.938	69.488
	Neck girth: caudal third	0.347	0.347	0.013	0.125	0.570
	Live body weight	0.088	0.088	0.000	0.054	0.121
Corrected Heart girth	Intercept	76.511	76.511	48.808	62.796	90.227
	Heart girth	−0.017	−0.017	0.001	−0.081	0.046
	Live body weight	0.111	0.111	0.000	0.092	0.130
Corrected Thigh circumference	Intercept	44.180	44.180	30.676	33.307	55.053
	Thigh circumference	0.217	0.217	0.007	0.059	0.376
	Live body weight	0.039	0.039	0.000	0.021	0.058
Corrected Hock circumference	Intercept	13.005	13.005	11.842	6.250	19.761
	Hock circumference	0.335	0.335	0.008	0.162	0.508
	Live body weight	0.025	0.025	0.000	0.015	0.036
Corrected Fore cannon bone perimeter	Intercept	10.646	10.646	2.169	7.755	13.537
	Fore cannon bone perimeter	0.247	0.247	0.005	0.104	0.390
	Live body weight	0.006	0.006	0.000	0.001	0.010
Corrected Rear cannon bone perimeter	Intercept	9.392	9.392	1.684	6.844	11.939
	Rear cannon bone perimeter	0.225	0.225	0.003	0.111	0.340
	Live body weight	0.009	0.009	0.000	0.005	0.013
Corrected Foot perimeter	Intercept	33.356	33.356	21.631	24.226	42.487
	Foot perimeter	0.260	0.260	0.016	0.015	0.506

Table 4. Bayes factor model summary for correction models comprising digital measurements and live body weight, except for foot perimeter, for which only digital measurement was used as a regressor, to estimate for on-field zoometric measurements in Canarian camels.

Zoometric Trait (=y)	Corrected Neck Girth: Caudal Third	Corrected Heart Girth	Corrected Thigh Circumference	Corrected Hock Circumference	Corrected Fore Cannon Bone Perimeter	Corrected Rear Cannon Bone Perimeter	Corrected Foot Perimeter
Correction Method	Bayesian regression and Natural logarithm	Bayesian regression and Natural logarithm	Bayesian regression	Bayesian regression and Natural logarithm	Bayesian regression and Natural logarithm	Bayesian regression and Natural logarithm	Bayesian regression and Natural logarithm
Regressors	Live body weight and Digital Imaging measurement for neck girth: caudal third	Live body weight and Digital Imaging measurement for heart girth	Live body weight and Digital Imaging measurement for Thigh circumference	Live body weight and Digital Imaging measurement for Hock circumference	Live body weight and Digital Imaging measurement for Fore cannon bone perimeter	Live body weight and Digital Imaging measurement for Rear cannon bone perimeter	Digital Imaging measurement for Foot perimeter
Round	3rd	3rd	2nd	3rd	3rd	3rd	3rd
Equation	y = 40.713 + 0.347 ∗ (Neck girth: caudal third) + 0.088 ∗ (Live body weight) + ln(Neck girth: caudal third)	y = 76.511 + (-0.017) ∗ (Heart girth) + 0.111 ∗ (Live body weight) +	y = 44.18 + 0.217 ∗ (Thigh circumference) + 0.039 ∗ (Live body weight)	y = 13.005 + 0.335(Hock circumference) + 0.025 ∗ (Live body weight) + ln(Hock circumference)	y = 10.646 + 0.247 ∗ (Fore cannon bone perimeter) + 0.006 ∗ (Live body weight) + ln(Fore	y = 9.392 + 0.225 ∗ (Rear cannon bone perimeter) + 0.009*(Live body weight) + ln(Rear	y = 33.356 + 0.260 ∗ (Foot perimeter) + ln(Foot perimeter)

		ln(Heart girth)			cannon bone perimeter)	cannon bone perimeter)	
Regression Sum of Squares	11,540.442	12,611.463	3226.575	1504.485	114.180	182.118	162.324
Regression df	2.000	2.000	2.000	2.000	2.000	2.000	1.000
Regression Mean Square	5770.221	6305.731	1613.288	752.242	57.090	91.059	162.324
F	20.168	67.975	23.580	33.454	11.409	23.354	4.409
Sig.	0.000	0.000	0.000	0.000	0.000	0.000	0.038
Residual Sum of Squares (RSS)	36,336.003	11,781.220	8689.017	2855.697	635.487	495.174	4712.808
Residual df	127.000	127.000	127.000	127.000	127.000	127.000	128.000
Residual Mean Square	286.110	92.766	68.417	22.486	5.004	3.899	36.819
Bayes Factor (BF)	269,937.547	6.39×10^{17}	3,356,913.557	2.93×10^{9}	252.807	2,850,184.198	0.597
R	0.491	0.719	0.520	0.587	0.390	0.519	0.182
Bayesian R Square	0.241	0.517	0.271	0.345	0.152	0.269	0.033
Bayesian Adjusted R Square	0.229	0.509	0.259	0.335	0.139	0.257	0.026
SE	16.915	9.631	8.271	4.742	2.237	1.975	6.068
Monte Carlo standard error (MCSE)	279.508	90.625	66.839	21.967	4.888	3.809	36.252
Bayesian Information Criterion (BIC)	95,207.940	76,173.431	71,028.278	52,222.907	26,827.621	22,611.369	60,684.398

LN: Natural logarithm; SE: Standard error.

Table 5. Predictive Posterior *p*-Values (pppvalues) for correction models comprising digital measurements and live body weight, except for foot perimeters, for which only digital measurement was used as a regressor to estimate for on-field zoometric measurements in Canarian camels.

Variables for Which a Correction Was Issued	P(T >= T_obs) Predictive Posterior *p*-Values
Corrected Neck girth: caudal third	0.496
Corrected Heart girth	0.459
Corrected Thigh circumference	0.495
Corrected Hock circumference	0.495
Corrected Fore cannon bone perimeter	0.494
Corrected Rear cannon bone perimeter	0.497
Corrected Foot perimeter	0.497
P(T >= T_obs) close to 0 or 1 indicates a lack of fit.	

3.4. Natural Logarithmic Correction for Perimeters and Girths and Third Round of Method Comparison/Repeatability and Scale Reliability

Afterwards, all the variables except for thigh perimeters had not reached acceptable levels of scale reliability (Average/Cα < 0.600, Table 2). Therefore, natural logarithm was added to their equation, and the third round of ICC computation was used.

3.5. Final Outputs for Method Comparison/Repeatability and Scale Reliability

After Bayesian linear regression modeling and natural logarithmic correction, all methods proved to be highly repeatable and reliable, as suggested by the values of ICC and 95% CI for average measurements (Average/Cα) for all the zoometric measurements that were made. Finally, the resulting equations are reported in Table 4. Linear zoometrics always reported excellent repeatability values over 0.836 (for sole length average measurements ICC) with high 95%CI lower bounds over 0.768. Although perimeters and girths

reported lower average measurements ICC, values were always higher than 0.654 (for foot perimeter average measurements ICC), which suggested good repeatability, while also presenting a reasonable 95%IC lower bound over 0.511. A summary of the results obtained after the three rounds of ICC calculation (single and average measurements/Cα) and 95%CI is reported in Table 1. Dispersion statistics for the measurements collected on-field and those extracted from digital imaging methods after correction are reported in Supplementary Table S3.

4. Discussion

Apart from the time reduction, personnel requirements, and handlers' safety improvement implicit in digital imaging zoometrics, a lower expected random error is obtained when these are compared to on-field measurements. This improved accuracy, reliability, and repeatability is not only supported by our results (Tables 2 and 5, Supplementary Table S3), but also by literature references highlighting a greater dispersion of the zoometric data collected with traditional instruments on-field against those extracted from digital image-based methods [5,8,88].

This may be ascribed to the difficulty for the animals to remain completely immobile during on-field measurement collection, which could add undesired noise to the data. As a drawback of image-based zoometric measurements, rigorous efforts may need to be made by operators to hold animals in the correct aplomb at a completely static position while keeping the photographic and camel midsagittal planes parallel [6].

In line with these preliminary arguments, collateral factors such as the image resolution, the accuracy of the distance measurement from the camera to the animal (focal plane), hair length and extension, coat color, and the fat condition of the animal, may need to be controlled before and during the zoometric measurements extraction from digital images to ensure that data depicts the real morphometry of the individuals as far as possible [8,19,89–91].

The correspondence between on-field and image-based zoometrics methods was evaluated via the average measurements intraclass correlation coefficient (ICC)/Cronbach's alpha (Cα) [92]. Method correspondence was considered acceptable when a limit value of 0.6 ICC/Cα was reached [93]. This limit was attained for all the measurements except for 'Neck girth: caudal third', 'Thoracic girth', 'Thigh perimeter', 'Hock perimeter', 'Fore cannon bone perimeter', 'Rear cannon bone perimeter', and 'Foot perimeter' at the first round (direct extrapolation). These findings were compared with those of Pezzuolo et al. [94] and Pérez-Ruiz et al. [89], who reported a particularly large relative error in digital three-dimensional zoometric measurements when compared to on-field three-dimensional measurements. Hence, the need for a correction methodology for digital three-dimensional measurements was suggested.

The basis for this lack of initial correspondence (in the first round) between three-dimensional measurements may be based on the fact that for their on-field collection, the participation of at least two operators is generally required. This, in turn, results in an unbalanced placement of the corresponding measuring instrument at different transverse planes in the homologous contralateral regions. By contrast, linear measurements are generally made by the same operator who controls the exact position of the instrument used for the measurement and is only performed on one side of the animal, which reduces the probability of finding morphological variance throughout the measured area.

As a result, the second round of correction was necessary to enhance method correspondence for the measurements for which acceptable levels had not been attained in the first round. A Bayesian linear regression was applied between manual and non-contact measurements, considering body weight as the most critical influencing parameter.

Evidence of body weight is a source for such quantitative differences between on-field and digital imaging-based three-dimensional measurements found, as suggested by the lack of evidence of significance and CV values. According to literature, the circular perimeter of the area to be measured can intrinsically vary along its length depending on

the regional adiposity [95] and the muscular development of the region [96], which are both directly related to body weight. Indeed, Boujenane [35] referenced that such a strong relationship between zoometry and weight could have been expected, since the estimation of the latter relies on chest and hump girth apart from height to withers via its estimation formula.

Once the digital measurement was multiplied by the coefficients obtained and the intercept value-added, the ICC between on-field and the corrected digital measurement improved only for the variable of 'Thigh perimeter'. Hence, the third round of correction was necessary to improve correspondence for the remaining measurements for which acceptable levels had not been reached. The correspondence between on-field and digital measurements was achieved after applying an additional correction consisting of the sum of the natural logarithm of the digital measurement (third round).

The fact that a linear regression model was enough to obtain a corrected digital measurement with acceptable correspondence for on-field thigh perimeter could be explained under the assumption that this area, given its location, hardly varies in its muscular tonus if no strong movements are carried out. This lack of variability does not distort skewness values; hence, the logarithmic correction does not improve correspondence values.

By contrast, for 'Neck girth: caudal third' and 'Thoracic girth', continuous respiratory movements may cause slight perimeter variations in the photographs taken during on-field evaluations, altering skewness properties and perhaps making it necessary to consider a natural logarithmic correction factor.

This could also be applied to the rest of the variables, that is, 'Hock perimeter, 'Fore cannon bone perimeter', 'Rear cannon bone perimeter', and 'Foot perimeter'. The implicit difficulty to restrain camels in a completely static position may induce temporary size changes in these local areas. Specifically, the pressure that the fore and rear limbs have to cope with depends on the particular position of the animal aplomb at the moment of measure collection (photo taking).

This may derive from the fact that the musculoskeletal systems involved in maintaining the posture are incapable of maintaining limbs in a perfect and unique stationary position, with the consequent increase in local muscle temperature due to rising blood flow and the transient oscillation of the distal limbs to the resonant frequency of heartbeats producing muscle tremor [97,98]. This translates into a source of increased skewness, data dispersion, and noise, which is corrected, as suggested by literature, via the addition of natural logarithms of the zoometric measurement to the equation.

5. Conclusions

The efficiency, repeatability, and accuracy of the on-field zoometric methods that are routinely considered for zoometric characterization in dromedaries can be enhanced through the use of digital imaging techniques. On-field and digital imaging zoometric extrapolation results in comparatively improved performance of the latter, due to the reduced dispersion of the data extracted from photographs. However, mathematical correction methods may be needed for three-dimensional measurements to reach acceptable levels of on-field/digital imaging methods correspondence. Body weight is the main source of bias in perimeter digital zoometric extraction if other factors such as age and coat color are controlled. All zoometric perimeters collected on-field should be regressed against body weight, except for foot perimeter, to ensure acceptable levels of correspondence are attained. Additionally, we summed the natural logarithms of the particular measurements which could be affected by spontaneous movements (breathing or proprioception) to correct for derived skewness distortion. The present method offers a time and economically affordable alternative, which saves the drawbacks derived from the lack of consideration of three-dimensional measurements that routinely occur in digital imaging zoometrics. The high degree of correspondence between methods makes this tool valid for its standardized implementation in camel zoometric characterization, while it may be translatable to other species.

References

1. Alhajeri, B.H.; Alaqeely, R.; Alhaddad, H. Classifying camel breeds using geometric morphometrics: A case study in Kuwait. *Livest. Sci.* **2019**, *230*, 103824.
2. Dorantes-Coronado, E.; Torres-Hernández, G.; Hernández-Mendo, O.; Rojo-Rubio, R. Zoometric measures and their utilization in prediction of live weight of local goats in southern México. *SpringerPlus* **2015**, *4*, 1–8.
3. Alhajeri, B.H.; Alhaddad, H.; Alaqeely, R.; Alaskar, H.; Dashti, Z.; Maraqa, T. Camel breed morphometrics: Current methods and possibilities. *Trans. R. Soc. S. Aust.* **2021**, *145*, 90–111.
4. Parés, C.; Sañudo, C. *Valoración Morfológica de Animales Domésticos*; Ministerio de Medio Ambiente y Medio Rural y Marino: Madrid, Spain, 2009.
5. Gaudioso, V.; Sanz-Ablanedo, E.; Lomillos, J.; Alonso, M.; Javares-Morillo, L.; Rodríguez, P. "Photozoometer": A new photogrammetric system for obtaining morphometric measurements of elusive animals. *Livest. Sci.* **2014**, *165*, 147–156.
6. Rahagiyanto, A.; Adhyatma, M. A Review of Morphometric Measurements Techniques on Animals Using Digital Image Processing. *Food Agric. Sci. Polije Proc. Ser.* **2021**, *3*, 67–72.
7. White, R.; Schofield, C.; Green, D.; Parsons, D.; Whittemore, C. The effectiveness of a visual image analysis (VIA) system for monitoring the performance of growing/finishing pigs. *Anim. Sci.* **2004**, *78*, 409–418.
8. Negretti, P.; Bianconi, G.; Finzi, A. Visual image analysis to estimate morphological and weight measurements in rabbits. *World Rabbit. Sci.* **2007**, *15*, 37–41.
9. De Wet, L.; Vranken, E.; Chedad, A.; Aerts, J.-M.; Ceunen, J.; Berckmans, D. Computer-assisted image analysis to quantify daily growth rates of broiler chickens. *Br. Poult. Sci.* **2003**, *44*, 524–532.
10. Bewley, J.; Peacock, A.; Lewis, O.; Boyce, R.; Roberts, D.; Coffey, M.; Kenyon, S.; Schutz, M. Potential for estimation of body condition scores in dairy cattle from digital images. *J. Dairy Sci.* **2008**, *91*, 3439–3453.
11. Azzaro, G.; Caccamo, M.; Ferguson, J.D.; Battiato, S.; Farinella, G.M.; Guarnera, G.C.; Puglisi, G.; Petriglieri, R.; Licitra, G. Objective estimation of body condition score by modeling cow body shape from digital images. *J. Dairy Sci.* **2011**, *94*, 2126–2137.
12. Cervantes, I.; Baumung, R.; Molina, A.; Druml, T.; Gutiérrez, J.; Sölkner, J.; Valera, M. Size and shape analysis of morphofunctional traits in the Spanish Arab horse. *Livest. Sci.* **2009**, *125*, 43–49.
13. Negretti, P.; Bianconi, G.; Bartocci, S.; Terramoccia, S.; Verna, M. Determination of live weight and body condition score in lactating Mediterranean buffalo by Visual Image Analysis. *Livest. Sci.* **2008**, *113*, 1–7.
14. O'Malley, B.P.; Schmitt, J.D.; Holden, J.P.; Weidel, B.C. Comparison of Specimen-and Image-Based Morphometrics for Cisco. *J. Fish Wildl. Manag.* **2021**, *12*, 208–215.
15. Shrader, A.M.; Ferreira, S.M.; Van Aarde, R.J. Digital photogrammetry and laser rangefinder techniques to measure African elephants. *S. Afr. J. Wildl.* **2006**, *36*, 1–7.
16. de Kock, M.E.; O'Donovan, D.; Khafaga, T.; Hejcmanová, P. Zoometric data extraction from drone imagery: The Arabian oryx (*Oryx leucoryx*). *Environ. Conserv.* **2021**, *48*, 295–300.

17. Proffitt, K.M.; Garrott, R.A.; Rotella, J.J.; Lele, S. Using form analysis techniques to improve photogrammetric mass-estimation methods. *Mar. Mammal Sci.* **2008**, *24*, 147–158.

18. de Bruyn, P.; Bester, M.; Carlini, A.; Oosthuizen, W. How to weigh an elephant seal with one finger: A simple three-dimensional photogrammetric application, *Aquat. Biol.* **2009**, *5*, 31–39.

19. Waite, J.N.; Schrader, W.J.; Mellish, J.-A.E.; Horning, M. Three-dimensional photogrammetry as a tool for estimating morphometrics and body mass of Steller sea lions (*Eumetopias jubatus*). *Can. J. Fish. Aquat. Sci.* **2007**, *64*, 296–303.

20. Bell, C.M.; Hindell, M.A.; Burton, H.R. Estimation of body mass in the southern elephant seal, Mirounga leonina, by photogrammetry and morphometrics. *Mar. Mammal Sci.* **1997**, *13*, 669–682.

21. Iglesias Pastrana, C.; Navas González, F.J.; Ciani, E.; Barba Capote, C.J.; Delgado Bermejo, J.V. Effect of research impact on emerging camel husbandry, welfare and social-related awareness. *Animals* **2020**, *10*, 780.

22. Al-Atiyat, R.M.; Suliman, G.; AlSuhaibani, E.; El-Waziry, A.; Al-Owaimer, A.; Basmaeil, S. The differentiation of camel breeds based on meat measurements using discriminant analysis. *Trop. Anim. Health Prod.* **2016**, *48*, 871–878.

23. Bitaraf Sani, M.; Hosseini, S.A.; Asadzadeh, N.; Ghavipanje, N.; Afshin, M.; Jasouri, M.; Banabazi, M.H.; Esmaeilkhanian, S.; Zare Harofte, J.; Shafei Naderi, A. A New Approach in the Evaluation of Dairy Camels: Using Test Day Milk and Morphometric Records. *Dairy* **2022**, *3*, 78–86.

24. Abdallah, H.R.; Faye, B. Phenotypic classification of Saudi Arabian camel (*Camelus dromedarius*) by their body measurements. *Emir. J. Food Agric.* **2012**, *24*, 272-280.

25. Meghelli, I.; Kaouadji, Z.; Yilmaz, O.; Cemal, İ.; Karaca, O.; Gaouar, S. Morphometric characterization and estimating body weight of two Algerian camel breeds using morphometric measurements. *Trop. Anim. Health Prod.* **2020**, *52*, 2505–2512.

26. Ayadi, M.; Aljumaah, R.S.; Samara, E.M.; Faye, B.; Caja, G. A proposal of linear assessment scheme for the udder of dairy camels (*Camelus dromedarius* L.). *Trop. Anim. Health Prod.* **2016**, *48*, 927–933.

27. Abdullahi, I.A.; Musa, H.A.-H.; Jibril, A. Scrotal circumference and testicular morphometric characteristics of the camel (*Camelus dromedarius*) in the semi-arid environment of northern Nigeria. *Int. J. Morphol.* **2012**, *30*, 1369–1372.

28. Köhler-Rollefson, I. Camel biodiversity—and how to conserve it. *Anim. Front.* **2022**, *12*, 17–19.

29. Iglesias Pastrana, C.; Navas González, F.J.; Ciani, E.; González Ariza, A.; Delgado Bermejo, J.V. A tool for functional selection of leisure camels: Behaviour breeding criteria may ensure long-term sustainability of a European unique breed. *Res. Vet. Sci.* **2021**, *140*, 142–152.

30. Çağlı, A.; Yılmaz, M. Determination of some body measurements of camels with three-dimensional modeling method (3D). *Trop. Anim. Health Prod.* **2021**, *53*, 1–12.

31. Gherissi, D.E.; Lamraoui, R.; Chacha, F.; Gaouar, S.B.S. Accuracy of Image Analysis for Linear Zoometric Measurements in Dromedary Camels. *Trop. Anim. Health Prod.* **2022**, *54*, 232-240.

32. Padalino, B.; Monaco, D.; Lacalandra, G.M. Male camel behavior and breeding management strategies: How to handle a camel bull during the breeding season? *Emir. J. Food Agric.* **2015**, *27*, 338–349.

33. Iglesias, C.; Navas, F.; Ciani, E.; Arbulu, A.A.; González, A.; Marín, C.; Mérida, S.N.; Bermejo, J.V.D. Zoometric characterization and body condition score in Canarian camel breed. *Arch. Zootec.* **2020**, *69*, 102–107.

34. Yakubu, A.; Ladokun, A.; Adua, M. Bioprediction of body weight from zoometrical traits of non-descript goats using linear and non-linear models in North Central Nigeria. *Livest. Res. Rural Dev.* **2011**, *23*, 6.

35. Boujenane, I. Comparison of body weight estimation equations for camels (*Camelus dromedarius*). *Trop. Anim. Health Prod.* **2019**, *51*, 1003–1007.

36. Babu, K. Natural textile fibres: Animal and silk fibres. In *Textiles and Fashion*; Elsevier: Amsterdam, The Netherlands, 2015; pp. 57–78.

37. Iglesias, C.; Navas, F.; Ciani, E.; Arando, A.; González, A.; Marín, C.; Nogales, S.; Delgado, J. Análisis biocinemático de locomoción y termografía aplicada en la raza camellar canaria. *Arch. Zootec.* **2020**, *69*, 102–107.

38. Puig-Diví, A.; Escalona-Marfil, C.; Padullés-Riu, J.M.; Busquets, A.; Padullés-Chando, X.; Marcos-Ruiz, D. Validity and reliability of the Kinovea program in obtaining angles and distances using coordinates in 4 perspectives. *PLoS ONE* **2019**, *14*, e0216448.

39. Bunting, K.V.; Steeds, R.P.; Slater, L.T.; Rogers, J.K.; Gkoutos, G.V.; Kotecha, D. A Practical Guide to Assess the Reproducibility of Echocardiographic Measurements. *J. Am. Soc. Echocardiogr.* **2019**, *32*, 1505–1515.

40. Fleiss, J.L.; Cohen, J. The equivalence of weighted kappa and the intraclass correlation coefficient as measures of reliability. *Educ. Psychol. Meas.* **1973**, *33*, 613–619.

41. Koo, T.K.; Li, M.Y. A Guideline of Selecting and Reporting Intraclass Correlation Coefficients for Reliability Research. *J. Chiropr. Med.* **2016**, *15*, 155–163.

42. Nunnally, J.C.; Bernstein, I. *The Role of University in the Development of Entrepreneurial Vocations: A Spanish Study*; McGraw-Hill: New York, NY, USA, 1994, 387–405.

43. Beanland, C.; Schneider, Z.; LoBiondo-Wood, G.; Haber, J. *Nursing Research: Methods, Critical Appraisal and Utilization*; Mosby: Maryland Heights, MI, USA, 1999.

44. Creswell, J.W. *Educational Research: Planning, Conducting, and Evaluating Quantitative*, 4th ed.; Prentice Hall Press: Upper Saddle River, NJ, USA, 2010.

45. George, D.; Mallery, P. Reliability analysis. *SPSS for Windows, Step by Step: A Simple Guide and Reference*, 14th Ed.; Allyn & Bacon: Boston, MA, USA, 2003; pp. 222–232.

46. Pallant, J. *SPSS Survival Manual: A Step by Step Guide to Data Analysis Using IBM SPSS*; Routledge: London, UK, 2020.

47. González Ariza, A.; Arando Arbulu, A.; Navas González, F.J.; Ruíz Morales, F.d.A.; León Jurado, J.M.; Barba Capote, C.J.; Camacho Vallejo, M.E. Sensory preference and professional profile affinity definition of endangered native breed eggs compared to commercial laying lineages' eggs. *Animals* **2019**, *9*, 920.

48. StataCorp. *Stata Statistical Software, 15*; StataCorp: College Station, TX, USA, 2017.

49. IBM Corp. *IBM SPSS Statistics for Windows*, 25.0; IBM Corp: Armonk, NY, USA, 2017.

50. Singaraju, G.S.; Js, Y.P.; Mandava, P.; Ganugapanta, V.R.; Teja, N.R.; Jn, P.R. Data Set for Computation of Maxillary Arch Perimeter with Ramanujan's Equation for Ellipse in Different Skeletal Malocclusions. *Data Br.* **2020**, *32*, 106079.

51. Alexander, M.; Kusleika, R. *Excel 2016 Formulas*; John Wiley & Sons: Hoboken, NJ, USA, 2016.

52. Chandrupatla, T.R.; Osler, T.J. The perimeter of an ellipse. *Math. Sci.* **2010**, *35*, 122–131.

53. Energy Information Administration of the United States. *Commercial Buildings Energy Consumption Survey: Commercial Buildings Energy Consumption and Expenditures*; Michigan State University: East Lansing, MI, USA, 1989.

54. Bao, L.; Gneiting, T.; Grimit, E.P.; Guttorp, P.; Raftery, A.E. Bias correction and Bayesian model averaging for ensemble forecasts of surface wind direction. *Mon. Weather Rev.* **2010**, *138*, 1811–1821.

55. Motulsky, H.J.; Brown, R.E. Detecting outliers when fitting data with nonlinear regression–a new method based on robust nonlinear regression and the false discovery rate. *BMC Bioinform.* **2006**, *7*, 123.

56. Carlin, J. Solutions to some exercises from Bayesian Data Analysis, by Gelman, Carlin, Stern, and Rubin. 2019.

57. Koehrsen, W. Introduction to Bayesian Linear Regression. An explanation of the Bayesian approach to linear modeling. *Towards Data Sci.* **2018**, *4*, 1.

58. Kundu, D. Bayesian inference and life testing plan for the Weibull distribution in presence of progressive censoring. *Technometrics* **2008**, *50*, 144–154.

59. IBM Corp. *IBM SPSS Statistics Algorithms*; IBM Corp: Armonk, NY, USA, 2017; p. 110.

60. MacKay, D. Information theory, pattern recognition and neural networks. In *Proceedings of the 1st International Conference on Evolutionary Computation*; Cambridge University Press: Cambridge, UK, 2003.

61. Brewer, K.R. *Combined Survey Sampling Inference: Weighing Basu's Elephants*; Oxford University Press: Oxford, UK, 2002.

62. Hayes, A.F.; Glynn, C.J.; Huge, M.E. Cautions Regarding the Interpretation of Regression Coefficients and Hypothesis Tests in Linear Models with Interactions. *Commun. Methods Meas.* **2012**, *6*, 1–11.

63. Liang, F.; Paulo, R.; Molina, G.; Clyde, M.A.; Berger, J.O. Mixtures of g priors for Bayesian variable selection. *J. Am. Stat. Assoc.* **2008**, *103*, 410–423.

64. Heck, D. A Caveat on the Savage-Dickey Density Ratio: The Case of Computing Bayes Factors for Regression Parameters. *Br. J. Math. Stat. Psychol.* **2019**, *72*, 316–333.

65. Zellner, A.; Siow, A. Posterior odds ratios for selected regression hypotheses. *Trab. Estadística Y Investig. Oper.* **1980**, *31*, 585–603.

66. Rouder, J.N.; Morey, R.D.; Speckman, P.L.; Province, J.M. Default Bayes factors for ANOVA designs. *J. Math. Psychol.* **2012**, *56*, 356–374.

67. Bayarri, M.J.; Berger, J.O.; Forte, A.; García-Donato, G. Criteria for Bayesian model choice with application to variable selection. *Ann. Stat.* **2012**, *40*, 1550–1577.

68. Rouder, J.N.; Morey, R.D. Default Bayes factors for model selection in regression. *Multivar. Behav. Res.* **2012**, *47*, 877–903.

69. Morey, R.; Rouder, J. BayesFactor 0.9. 12-2. Comprehensive R Archive Network. 2015.

70. Rouder, J.N.; Speckman, P.L.; Sun, D.; Morey, R.D.; Iverson, G. Bayesian t tests for accepting and rejecting the null hypothesis. *Psychon Bull. Rev.* **2009**, *16*, 225–237.

71. Depaoli, S.; Van de Schoot, R. Improving transparency and replication in Bayesian statistics: The WAMBS-Checklist. *Psychol. Methods* **2017**, *22*, 240.

72. Kass, R.E.; Raftery, A.E. Bayes factors. *J. Am. Stat. Assoc.* **1995**, *90*, 773–795.

73. Arora, J.S. Chapter 14—Practical Applications of Optimization. In *Introduction to Optimum Design*, 14th ed.; Arora, J.S., Ed.; Academic Press: Boston, MA, USA, 2017; pp. 601–680.

74. Pizarro Inostroza, M.G.; Navas González, F.J.; Landi, V.; León Jurado, J.M.; Delgado Bermejo, J.V.; Fernández Álvarez, J.; Martínez Martínez, M.d.A. Bayesian Analysis of the Association between Casein Complex Haplotype Variants and Milk Yield, Composition, and Curve Shape Parameters in Murciano-Granadina Goats. *Animals* **2020**, *10*, 1845.

75. Geweke, J. *Variable Selection and Model Comparison in Regression*; Working Papers 539; Federal Reserve Bank of Minneapolis: Minnesota, MI, USA, 1996.

76. Analla, M. Model validation through the linear regression fit to actual versus predicted values. *Agric. Syst.* **1998**, *57*, 115–119.

77. Doğan, N.Ö. Bland-Altman analysis: A paradigm to understand correlation and agreement. *Turk. J. Emerg. Med.* **2018**, *18*, 139–141.

78. Pizarro Inostroza, M.G.; Navas González, F.J.; Landi, V.; León Jurado, J.M.; Delgado Bermejo, J.V.; Fernández Álvarez, J.; Martínez Martínez, M.d.A. Software-Automatized Individual Lactation Model Fitting, Peak and Persistence and Bayesian Criteria Comparison for Milk Yield Genetic Studies in Murciano-Granadina Goats. *Mathematics* **2020**, *8*, 1505.

79. Pizarro Inostroza, M.G.; Navas González, F.J.; Landi, V.; León Jurado, J.M.; Delgado Bermejo, J.V.; Fernández Álvarez, J.; Martínez, M.d.A.M. Goat Milk Nutritional Quality Software-Automatized Individual Curve Model Fitting, Shape Parameters Calculation and Bayesian Flexibility Criteria Comparison. *Animals* **2020**, *10*, 1693.

80. Hall, P.; Maiti, T. Nonparametric estimation of mean-squared prediction error in nested-error regression models. *Ann. Stat.* **2006**, *34*, 1733–1750.

81.   Jeffreys, H. *Theory of Probability*, 3rd ed.; Oxford University Press: Oxford, UK, 1961.
82.   Lee, M.; Wagenmakers, E. *Bayesian Data Analysis for Cognitive Science: A Practical Course*; Cambridge University Press: New York, NY, USA, 2013.
83.   Kaplan, D.; Depaoli, S. Bayesian structural equation modeling. In *Handbook of Structural Equation Modeling*; Hoyle, R.H., Ed.; The Guilford Press: New York, NY, USA, 2012; pp. 650–673.
84.   Gelman, A.; Carlin, J.B.; Stern, H.S.; Dunson, D.B.; Vehtari, A.; Rubin, D.B. *Bayesian Data Analysis*; CRC Press: Boca Ratón, FL, USA, 2013.
85.   Drton, M.; Plummer, M. A Bayesian information criterion for singular models. *J. R. Stat. Soc. Series. B Stat. Methodol.* **2017**, *79*, 323–380.
86.   Clyde, M.; Cetinkaya-Rundel, M.; Rundel, C.; Banks, D.; Chai, C.; Huang, L. Chapter 7. Bayesian Model Choice. In *An Introduction to Bayesian Thinking*; BookDown; CRC Press; Boca Ratón, FL, USA, 2019.
87.   Gelman, A.; Goodrich, B.; Gabry, J.; Vehtari, A. R-squared for Bayesian regression models. *Am. Stat.* **2019**, *73*, 307–309.
88.   Huang, L.; Li, S.; Zhu, A.; Fan, X.; Zhang, C.; Wang, H. Non-contact body measurement for qinchuan cattle with LiDAR sensor. *Sensors* **2018**, *18*, 3014.
89.   Pérez-Ruiz, M.; Tarrat-Martín, D.; Sánchez-Guerrero, M.J.; Valera, M. Advances in horse morphometric measurements using LiDAR. *Comput. Electron. Agric.* **2020**, *174*, 105510.
90.   Muir, A.; Vecsei, P.; Pratt, T.; Krueger, C.; Power, M.; Reist, J. Ontogenetic shifts in morphology and resource use of cisco *Coregonus artedi*. *J. Fish Biol.* **2013**, *82*, 600–617.
91.   Collins, K.S.; Gazley, M.F. Does my posterior look big in this? The effect of photographic distortion on morphometric analyses. *Paleobiology* **2017**, *43*, 508–520.
92.   Colli, L.; Perrotta, G.; Negrini, R.; Bomba, L.; Bigi, D.; Zambonelli, P.; Verini Supplizi, A.; Liotta, L.; Ajmone-Marsan, P. Detecting population structure and recent demographic history in endangered livestock breeds: The case of the Italian autochthonous donkeys. *Anim. Genet.* **2013**, *44*, 69–78.
93.   Abu-Zidan, F.M.; Eid, H.O.; Hefny, A.F.; Bashir, M.O.; Branicki, F. Camel bite injuries in United Arab Emirates: A 6 year prospective study. *Injury* **2012**, *43*, 1617–1620.
94.   Pezzuolo, A.; Guarino, M.; Sartori, L.; Marinello, F. A feasibility study on the use of a structured light depth-camera for three-dimensional body measurements of dairy cows in free-stall barns. *Sensors* **2018**, *18*, 673.
95.   Jensen, R.B.; Danielsen, S.H.; Tauson, A.-H. Body condition score, morphometric measurements and estimation of body weight in mature Icelandic horses in Denmark. *Acta Vet. Scand.* **2016**, *58*, 19–23.
96.   Albertí, P.; Ripoll, G.; Goyache, F.; Lahoz, F.; Olleta, J.; Panea, B.; Sañudo, C. Carcass characterisation of seven Spanish beef breeds slaughtered at two commercial weights. *Meat Sci.* **2005**, *71*, 514–521.
97.   Lakie, M. The influence of muscle tremor on shooting performance. *Exp. Physiol.* **2010**, *95*, 441–450.
98.   Marsden, C.; Meadows, J.; Lange, G.; Watson, R. The role of the ballistocardiac impulse in the genesis of physiological tremor. *Brain* **1969**, *92*, 647–662.